MATHEMATICAL MODELING AND SIMULATION OF THE SPACE SHUTTLE IMAGING RADAR ANTENNAS

ROSS W. CAMPBELL, KAREN E. MELICK, AND EDGAR L. COFFEY, III
PHYSICAL SCIENCE LABORATORY
NEW MEXICO STATE UNIVERSITY
LAS CRUCES, NEW MEXICO 88001

SUMMARY

Simulations of Space Shuttle synthetic aperture radar antennas under the influence of space environmental conditions have been carried out at L, C, and X-band. Mathematical difficulties in modeling large, non-planar array antennas are discussed, and an approximate modeling technique is presented. Results for several antenna error conditions are illustrated in far-field profile patterns, earth surface footprint contours, and summary graphs.

1.0 INTRODUCTION

Antennas to be used on Space Shuttle missions in the 1980's for synthetic aperture radars are expected to undergo stresses induced by the space environment that may degrade the performance of the radar. For example, thermal gradients across and through the antenna surface may cause the structure to bow. Deployment techniques that rely on unfolding the antenna in one or more places may create surface discontinuities at the fold joints. in addition, feedline lengths may change slightly due to thermal expansion, resulting in phase excitation errors. Power division to different sections of the antenna may be perturbed by non-unity VSMRs. To estimate the effect of these and other antenna errors on overall synthetic aperture radar performance, it is necessary to computer simulate the antenna over a wide range of possible error conditions. Unfortunately, classical methods of analysis, such as computing the array factor as the weighted sum of path length differences, are unmanageable because of the large electrical size of the antenna. A closed-form array factor expression is unobtainable because of the general nature of the mechanical surface errors. To overcome these computational limitations, a compromise modeling method was developed.

2.0 THE MATHEMATICAL MODEL

2.1 MODEL OF MECHANICAL SURFACE FLATNESS ERRORS

The physical array surface is modeled with a number of piecewise bilinear rectangular sections as illustrated in Figure 1. That is, if the array is nominally located in the (x,y)-plane, the z-axis displacement of the array surface is given by

$$z(x,y) = \sum_{m=1}^{M} z_m(x,y) \tag{1}$$

where

$$z_m(x,y) = \begin{cases} a_0^m + a_1^m x_m + a_2^m y_m + a_3^m x_m y_m \text{ in the } m^{th} \text{ section} \\ 0 \text{ elsewhere} \end{cases} \tag{2}$$

and (x_m,y_m) are the local coordinates of the m^{th} section shown in Figure 2. The $\{a_n^m\}$ coefficients may be determined uniquely from the displacements at each of the four corners of the rectangle. Furthermore, the same coefficients give a continuous approximation of the actual antenna surface. These sections need not conform to physical antenna panels. The number of sections needed can be determined by the curvature of the warped surface and the maximum error that can be tolerated. As the number of sections is increased, the approximation becomes more exact, converging to the actual surface in the limit. [4] Of course, the results become exact electrically when each section contains only one element of the array.

2.2 MODEL OF ELECTRICAL ERRORS

Let us suppose the array antenna is divided into M x N subarray sections as illustrated in Figure 3. The far-field pattern of such an antenna may be written as the weighted sum of the contributions from each subarray.

$$\bar{E}(r,\theta,\phi) = \frac{j\beta\eta}{4} \frac{e^{-j\beta r}}{r} \sum_{m=1}^{M} \sum_{n=1}^{N} a_{mn} e^{j\phi_{mn}} \bar{g}_{mn}(u,v)\, e^{j\Psi} \tag{3}$$

where: $a_{mn}e^{j\phi_{mn}}$ = the complex excitation of the mn^{th} subarray

(u,v,w) = $(\sin\theta\cos\phi, \sin\theta\sin\phi, \cos\theta)$, the cosines of the beam pointing direction with respect to the x, y, and z axes

$\beta = 2\pi/\lambda$ = wave number of the source

$\eta = \sqrt{\frac{\mu}{\epsilon}}$ = intrinsic impedance of the medium

$\bar{g}_{mn}(u,v)$ = vector array factor of the mn^{th} subarray

Ψ = $(x_{mn}u + y_{mn}v + z_{mn}w)$

(x_{mn},y_{mn},z_{mn}) = location of the center of the mn^{th} subarray

If the vector subarray factor is known, equation (3) may be used to obtain the far-field pattern. Either measured data or computed data may be used for g(u,v).

Each electrical section may be excited separately in both magnitude and phase. The number of sections needed to obtain a desired accuracy is determined by the severity of the electrical taper.

2.3 SIMULTANEOUS MECHANICAL AND ELECTRICAL ERRORS

If the bilinear rectangular sections of (2.1) are made to conform with the subarray sections of (2.2), then electrical and mechanical errors may be studied simultaneously. The only further approximation needed is in the computation of the subarray factor $\bar{g}(u,v)$ for elements equally spaced over a bilinear surface. A closed-form expression for $\bar{g}$ is not available; however, since all sections are the same physical size, $\bar{g}$ could be computed and tabulated parametrically so that when using equation (3), only a table look-up is necessary.

If the bilinear surfaces are sufficiently flat, an alternative technique is available. The two straight lines formed by projecting the localized coordinate axes onto the bilinear surface of (2) may be used to define an error-minimizing plane.[1] That is, the coefficients of

$$z_m(x_m,y_m) = b_o^m + b_1^m x_m + b_2^m y_m \tag{4}$$

are chosen so that the error

$$\varepsilon = \iint_{\text{section}} |(a_o = a_1 x + a_2 y + a_3 xy) - (b_o + b_1 x + b_2 y)| dxdy \tag{5}$$

is a minimum. The superscript "m" has been omitted for clarity. The minimum occurs when

$$\begin{aligned} b_o &= a_o \\ b_1 &= a_1 \\ b_2 &= a_2 \end{aligned} \tag{6}$$

and the integrated error $\varepsilon = A^2/16 * |a_3|$, where A is the surface area of one rectangle. A maximum error of $A/4 * |a_3|$ occurs at the corners of the rectangle. Consequently, the subarray factor used in calculations is the pattern from a planar rectangular array with average displacement

$$z_{avg} = b_0 \tag{7}$$

whose normal points in the direction (θ_m,ϕ_m) defined by

$$\begin{aligned} \tan(\alpha_x^m) &= b_1^m \\ \tan(\alpha_y^m) &= b_2^m \end{aligned} \tag{8}$$

where

$$\cos(\alpha_x^m) = \sin(\theta_m)\cos(\phi_m)$$
$$\cos(\alpha_y^m) = \sin(\theta_m)\cos(\phi_m) \qquad (9)$$

The array factor for each subarray is the well-known

$$\frac{\sin\frac{M\Psi x}{2}}{M\sin\frac{\Psi x}{2}} \cdot \frac{\sin\frac{N\Psi y}{2}}{N\sin\frac{\Psi y}{2}} \qquad (10)$$

pattern with the angular tilt due to α_x and α_y included in the Ψ-factors.

3.0 SIMULATION RESULTS

A variety of antenna mechanical surface errors and electrical excitation errors have been simulated at 1.5, 4.5, 9.0, 12.0 and 14.0 GHz [2,3], including:

- Antenna panel unfolding errors due to incomplete deployment of a folded panel.
- Various warping conditions due to thermal gradients through the antenna surface.
- Electrical excitation errors occurring from feedline mismatches.

For the antenna panel unfolding errors, a three-panel array was modeled with the outer two panels tilted away from the perfectly flat baseline case. Deflections varied from 0.5 cm to 5.0 cm over the 11.6 m length of the entire array. Figure 3 consists of four graphs which illustrate gain degradation versus frequency, gain degradation versus warp severity, beam pointing error versus warp severity, and side lobe level versus wrap severity.

Parabolic bow mechanical errors caused by the thermal gradients through the antenna were modeled with a twelve-panel array curved to fit a parabola (in azimuth) with maximum deflection ranging from 1 cm to 5 cm. Figure 4 consists of four graphs which depict the aximuth far-field pattern of a uniformly excited 11.6 m antenna at 1.5 GHz for bows of 1.0, 2.0, 3.0, and 4.0 cm. Two-dimensional Earth surface footprints for the parabolic bow error as well as the unfolding error are shown in Figure 5.

Electrical mismatch errors were studied for the seven panel SIR-A microstrip array antenna for VSWRs of 1.0, 1.1, and 1.2. Results are shown in Figure 6.

4.0 REFERENCES

[1] E. L. Coffey, Interim Report on Antenna Evaluation for the Shuttle Imaging Radar: Phase I (NASA Contract NAS9-95469), Physical Science Laboratory Report No. PA00853, New Mexico State University, Las Cruces, NM, July 1976.

[2] E. L. Coffey and K. R. Carver, Final Report on Antenna Evaluation Study for the Shuttle Multispectral Radar: Phase I (NASA Contract NAS9--5469), Physical Science Laboratory Report No. PA00874, New Mexico State University, Las Cruces, NM, December 1976.

[3] E. L. Coffey and K. R. Carver, Final Report on Antenna Evaluation Study for the Shuttle Multspectral Radar: Phase II (NASA Contract NAS9-95471), Physical Science Laboratory Report No. PA00881, New Mexico State University, Las Cruces, NM, May 1977.

[4] G. Strong and G. J. Fix, An Analysis of the Finite Element Method, Prentice - Hall, New York, 1973, pp. 165-171.

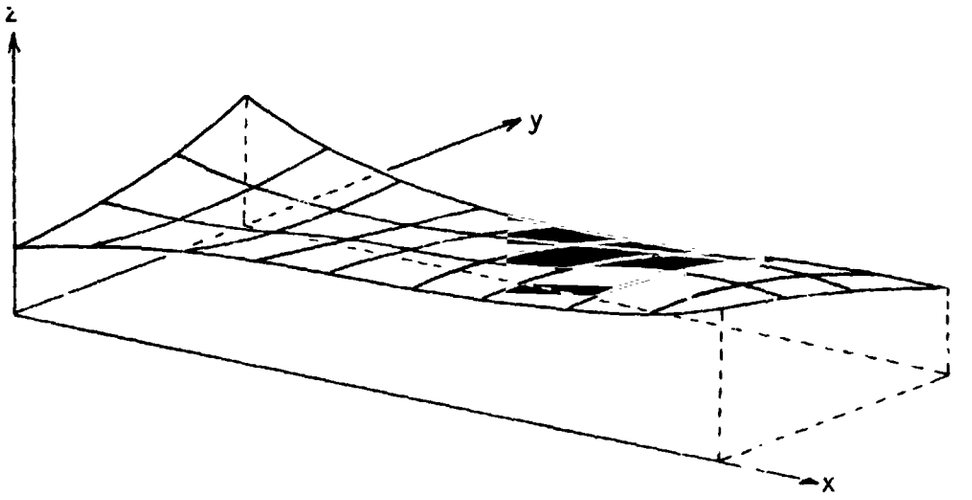

Figure 1a. Mechanically deformed array surface.

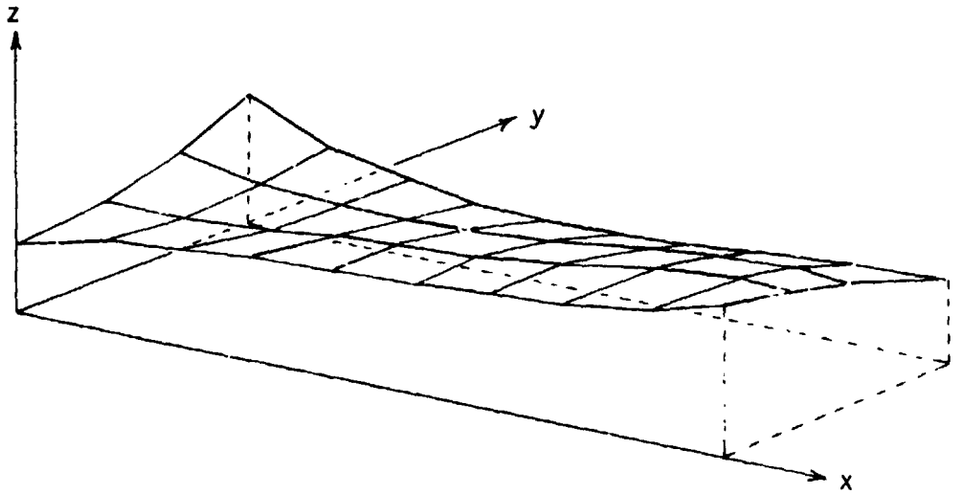

Figure 1b. Piecewise bilinear approximation.

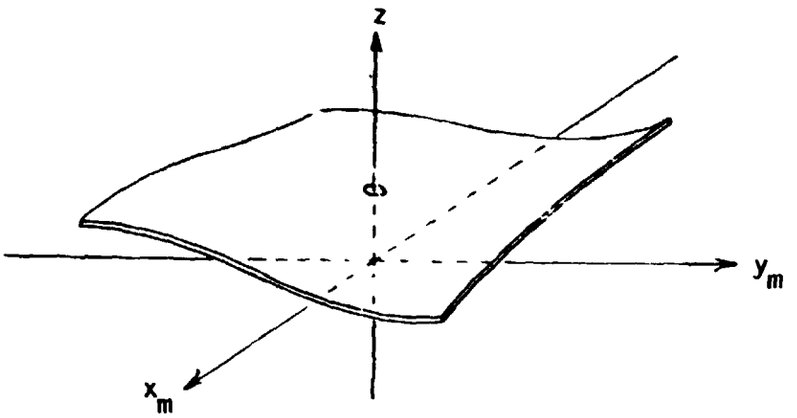

Figure 2a. Original surface.

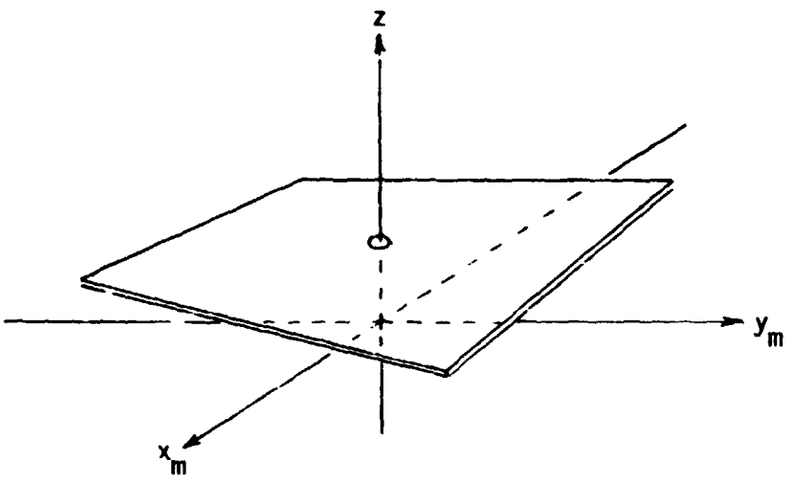

Figure 2b. Bilinear approximation.

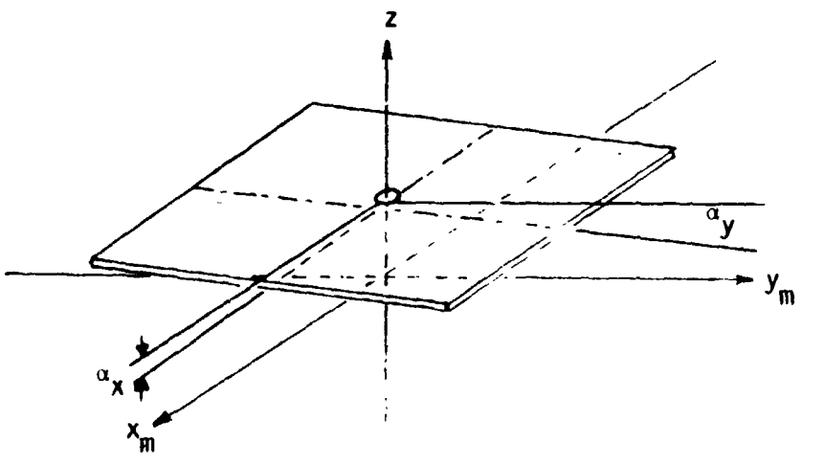

Figure 2c. Planar approximation.

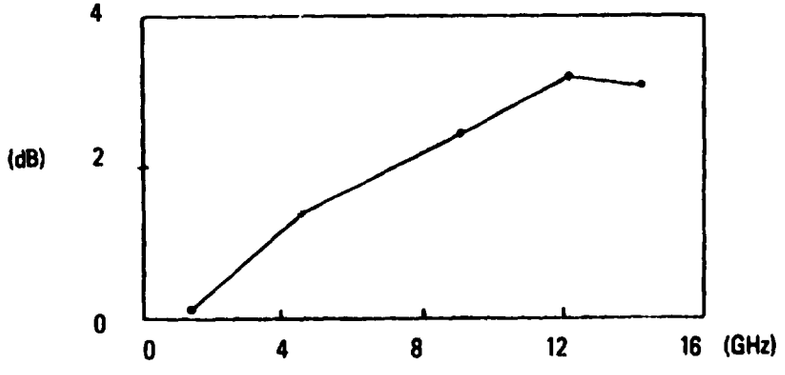

Gain Degradation (dB) vs. Frequency (GHz)
(Panel Unfolding Error: -1.0, 2.0 cm), 50 deg. tilt

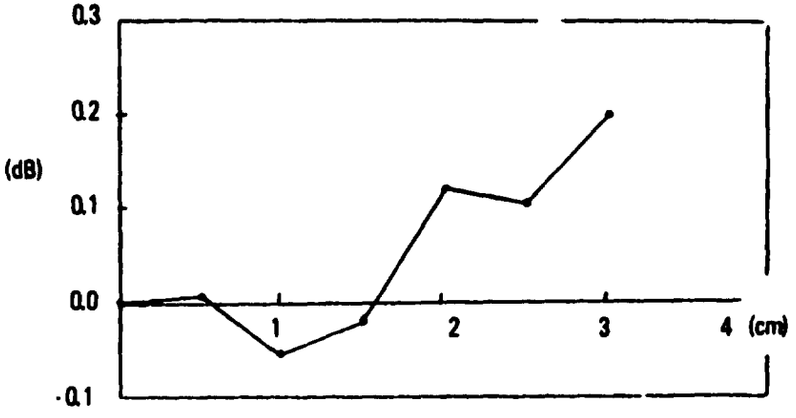

Gain Degradation (dB) vs. Warp Severity (cm) at 1.5 GHz,
10 deg. Tilt, Panel Unfolding Errors

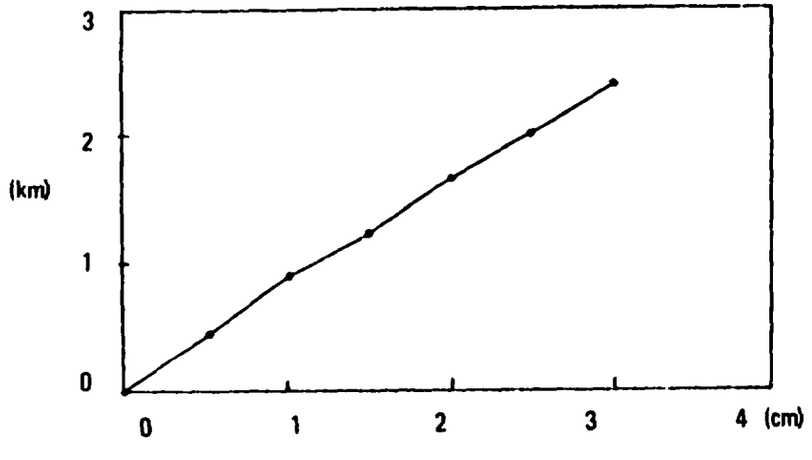

Beam Pointing Error (km) vs. Panel Unfolding Error (cm)
at 1.5 GHz, 50 deg. tilt.

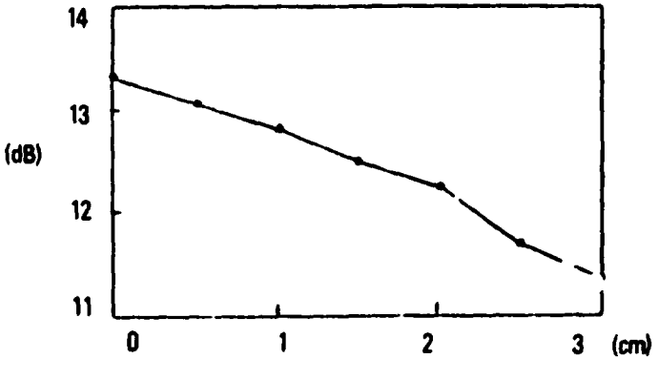

Azimuth Profile Plane Side Lobe Level (dB) vs. Warp Severity
(cm) for Panel Unfolding Errors at 1.5 GHz., 50 deg. tilt

Figure 3.

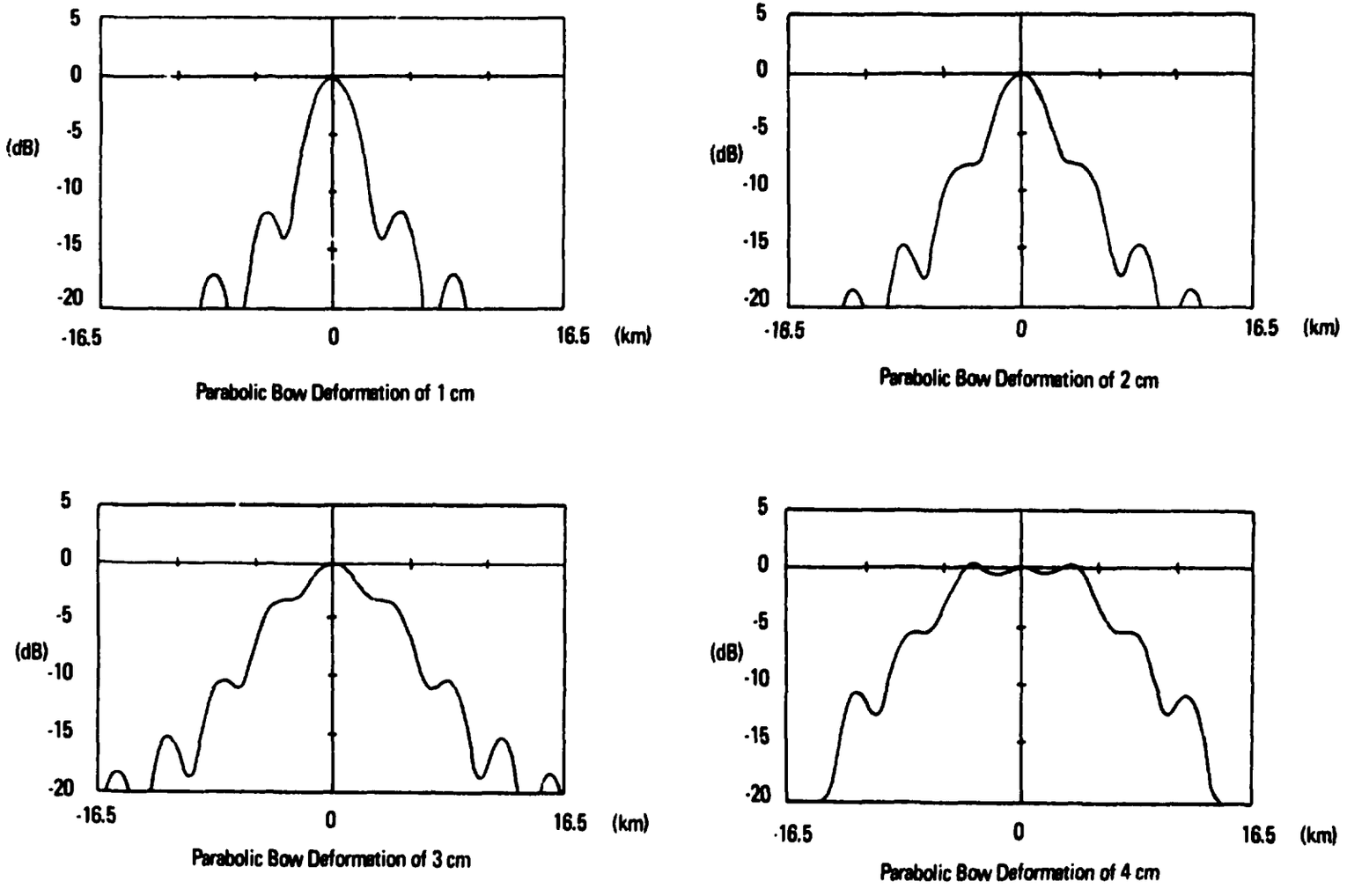

Figure 4. Azimuth Main Beam Profile vs. Longitudinal Distance: f = 1.5 GHz, Tilt = 50 deg., and altitude = 200 km.

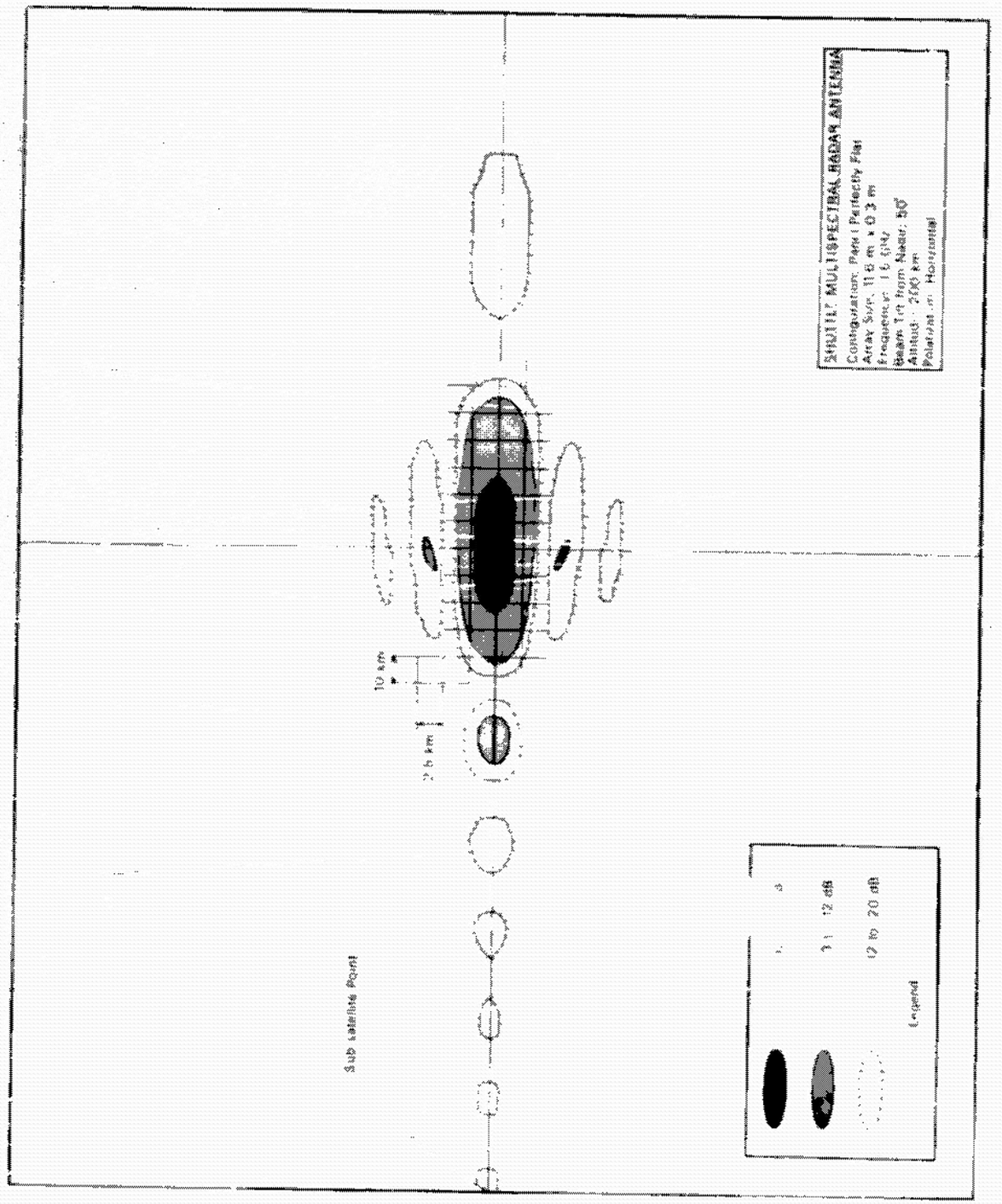

Figure 5a. Earth Surface Footprint - Panel Perfectly Flat.

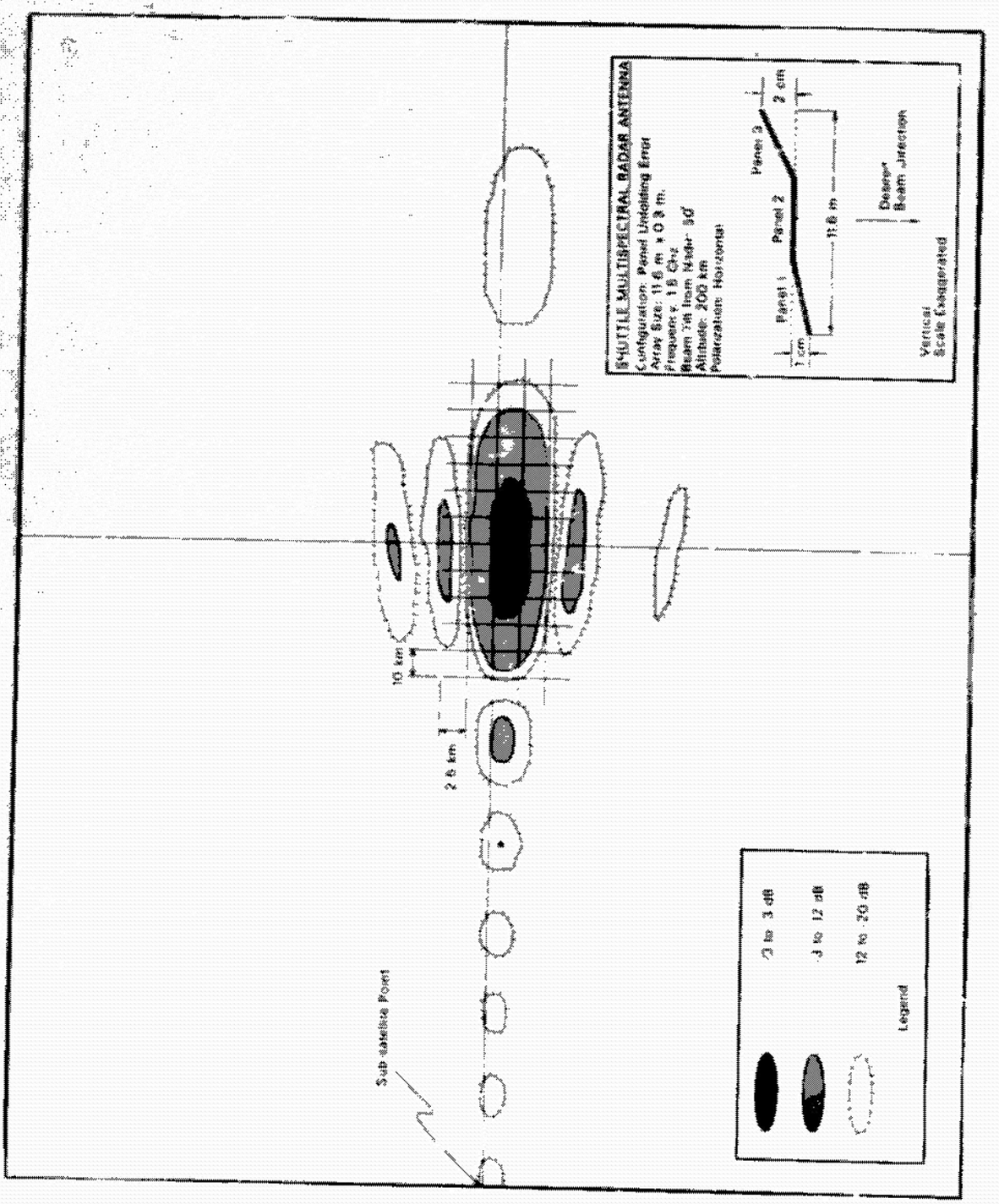

Figure 5b. Earth Surface Footprint - Panel Unfolding Error.

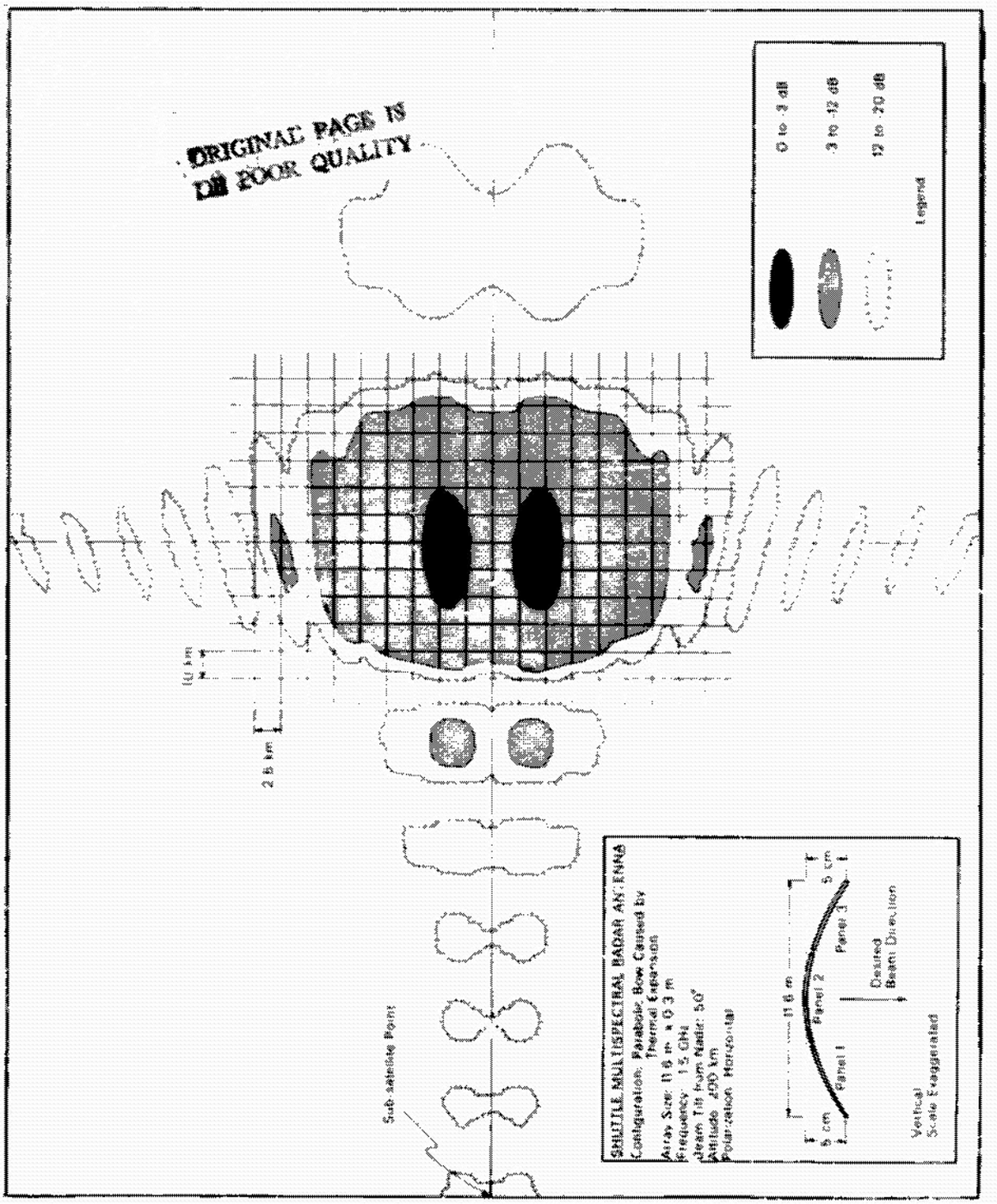

Figure 5c. Earth Surface Footprint - Parabolic Bow Error.

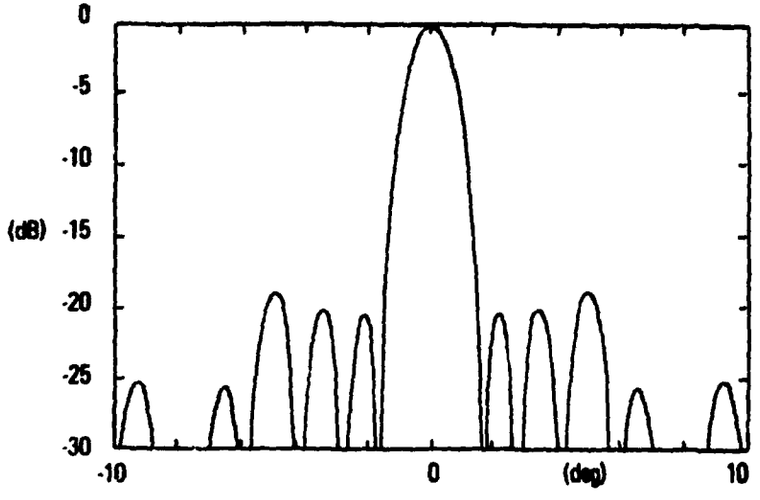

Figure 6a.

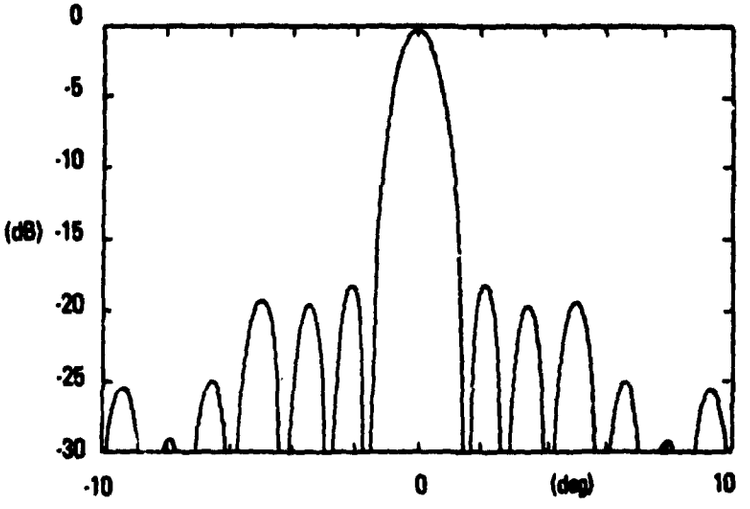

Figure 6b.

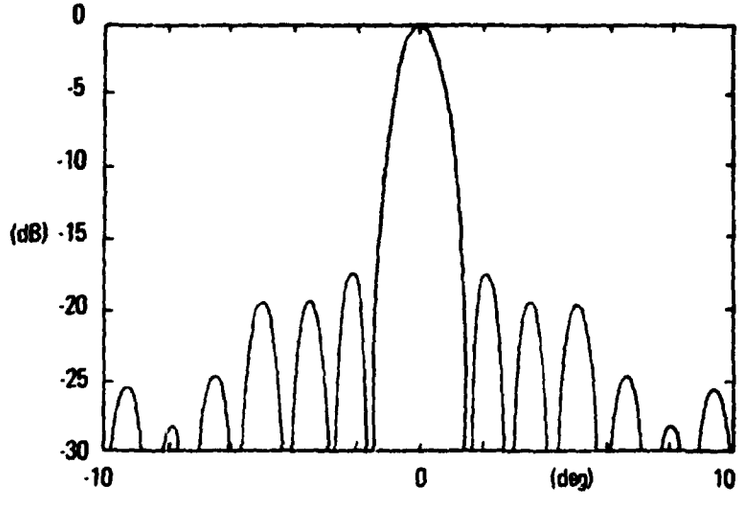

Figure 6c.

Figure 6a. SIR-A Antenna, Azimuth taper=1.5, VSWR = 1:1, Baseline configuration.

Figure 6b. SIR-A Antenna, Azimuth taper=1.5, VSWR = 1.1:1, Baseline configuration.

Figure 6c. SIR-A Antenna, Azimuth taper=1.5, VSWR = 1.2:1, Baseline configuration